Influence of light on spin diffusion in weak magnetic fields

J.-H. Quast, G. V. Astakhov,* W. Ossau, and L. W. Molenkamp
Physikalisches Institut (EP3), Universität Würzburg, 97074 Würzburg, Germany

J. Heinrich, S. Höfling, and A. Forchel
Physikalisches Institut (TP), Universität Würzburg, 97074 Würzburg, Germany

(Received 20 May 2009; published 24 June 2009)

We demonstrate that optical illumination strongly influences spin transport in *n*-type GaAs. Specifically, increasing the power density of optical spin pumping results in a significant expansion of the spin-diffusion profile. A further means of manipulation is the application of a weak transverse magnetic field, which strongly increases the spin flow out of the excitation spot. These effects are directly monitored in spin-imaging experiments and spatially resolved Hanle measurements.

DOI: 10.1103/PhysRevB.79.245207 PACS number(s): 72.25.Dc, 72.25.Fe, 72.25.Rb, 85.75.−d

The ability to monitor, control, and manipulate spin flows in semiconductors is a prerequisite for the functionality of spin-based devices. Because of the spin selectivity of the selection rules,[1] optical spectroscopy has emerged as a powerful tool to locally probe the spin of electrons. Spin diffusion lengths of over approximately 10 μm in *n*-GaAs (Ref. 2) and spin drag over 100 μm (Ref. 3) enable optical detection of spin injection,[4–8] spin accumulation,[7] and the spin-Hall effect.[9] In this type of experiments, the optical-excitation density is kept low in order to minimize a possible perturbation of the spin system, implicitly assuming that using a low optical-power density implies that the dilution of intrinsic electrons in the semiconductor with photogenerated ones can be neglected. Generally, this condition is met when $G\tau < n_e$, where G is the generation rate (which is proportional to the illumination power density), τ is the lifetime of the photogenerated carriers, and n_e is the concentration of intrinsic electrons. However, for a spin-polarized electron system, recombination with photogenerated holes will reduce the spin polarization. This additional effect becomes relevant when $G\tau_s > n_e$, where τ_s now is the electron-spin relaxation time.[1] Therefore, in semiconductors with a very long electron-spin memory, i.e., when $\tau_s \gg \tau$, this mechanism may lead to enhanced spin decay at quite low pump/probe-power densities and hence should not be neglected *a priori*. On the plus side, this same mechanism can be used to locally control spin flow even without application of a bias voltage, as we will demonstrate below.

In brief, laser light introduces a spatial variation in the spin lifetime (T_s) and thus the suppression of spin polarization in a transverse magnetic field (known as the Hanle effect[1]) becomes spatially dependent. In particular, stronger spin pumping results in a shorter spin lifetime and thus a stronger magnetic field is required to suppress the spin polarization within the pump spot, while outside the pump spot the spin polarization reduces more quickly with rising fields. As a result, in weak magnetic fields (a few tens of Gauss) the spin gradient (and therefore the spin flow out of the injection area) increases.

We present results for a Si-doped *n*-type GaAs layer ($n_e = 2.5 \times 10^{16}$ cm^{-3}) of $d = 1.5$ μm thickness. It was grown by molecular-beam epitaxy (MBE) on semi-insulating (001) GaAs substrate followed by an undoped 200 nm GaAs buffer, a 5 nm AlAs barrier, and an undoped 100 nm GaAs spacer layer. The sample is mounted strainfree and kept at a temperature $T = 8$ K. In order to perform optical spin pumping and probing we use a two-color Kerr rotation technique.[10] Optical excitation is performed by a solid-state laser (785 nm) modulated between σ^+ and σ^- circular polarizations at a frequency of 50 kHz. The net spin polarization along z direction S_z is probed using the magneto-optical Kerr effect (MOKE). The photoinduced Kerr rotation θ of a Ti:sapphire laser (819 nm) which is proportional to the spin polarization ($\theta \propto S_z$) is measured by balanced photodiodes and demodulated by a lock-in amplifier. Scanning Kerr microscopy is used to spatially resolve the net spin polarization.[3,11] The experimental scheme is depicted in Fig. 1(a). In this technique, a circularly polarized pump beam is directed under a 45° angle of incidence (within the *y*-*z* plane) to the sample surface (*x*-*y* plane). After refraction inside the sample the pump beam generates spins polarized at an angle $\gamma = 11°$ with respect to the sample normal (z direction). Surface scans in the *x*-*y* plane are performed using a microscope objective (NA=0.14) mounted on a piezo system. Another microscope objective of the same kind is used to focus the pump beam. External magnetic fields up to 100 mT, provided by an electromagnet, are applied in the sample plane (along the x axis). The spatial resolution of our setup can be inferred from a scan of the transmission of the focused laser beam over a sharp edge as shown in Fig. 1(b). The derivative of this trace (inset) confirms that the spot profile has the form $\exp(-x^2/\Delta_p^2)$ with $\Delta_p = 3.3$ μm; we have verified that the profile in the sharp-edge scans is circular.

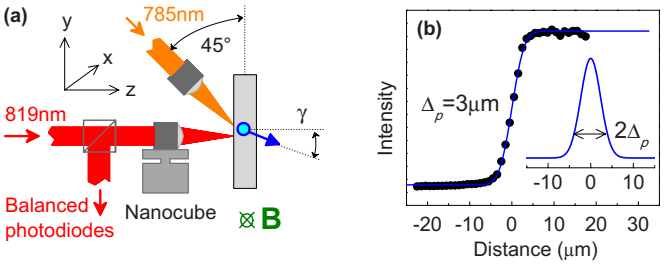

FIG. 1. (Color online) (a) Schematic of the two-color Kerr microscopy setup. (b) Scan of the laser spot through a sharp edge. The line is a fit of an error function. Inset: laser spot profile obtained from this fit.

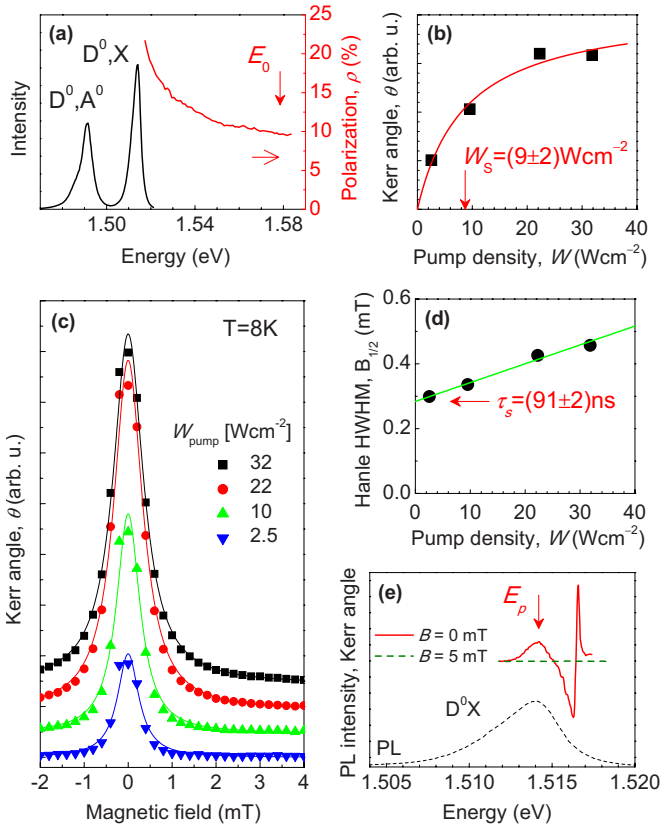

FIG. 2. (Color online) Sample characterization in a configuration where spin diffusion is averaged out. (a) PL and polarization excitation spectra. (b) Kerr rotation vs pump-power density. Solid line is a fit to Eq. (1). (c) Hanle curves for different pump-power densities. Solid lines represent fits to Eq. (2). The curves are shifted for clarity. (d) Hanle HWHM $B_{1/2}$ vs pump-power density W. The solid line is a fit to Eq. (3). (e) Kerr angle θ vs probe energy E_p. Pump energy is $E_0=1.58$ eV.

First, we characterize the sample in an excitation configuration where spin diffusion is averaged out (Fig. 2), using two-color Kerr and photoluminescence (PL) measurements. Instead of the microscope objectives, we employ two long-focus lenses to provide spot radii of about 100 μm which is much larger than the typical spin-diffusion length. The PL spectrum consists of two bands which we attribute to donor-acceptor (D^0,A^0) transitions and donor-bound excitonic (D^0,X) recombination [see Fig. 2(a)]. In the same figure, we plot the optically induced circular polarization ρ_c of the PL [detected at (D^0,X) band], as a function of the excitation energy. A maximum value of $\rho_c=22$ % [the theoretical limit is 25% (Ref. 1] is achieved for quasiresonant excitation. The vertical arrow in Fig. 2(a) indicates the pump energy $E_0=1.58$ eV which has been used in all further experiments. The Kerr angle θ is proportional to the net spin polarization S_z. The amplitude of the polarization depends on pump power; θ increases linearly for low and saturates for high pump-power density, as shown in Fig. 2(b). This behavior can be well described by[1]

$$S_z(W) = \frac{S_{z0}}{1 + W_S/W}. \tag{1}$$

Here, $W_S=(9\pm2)$ W cm^{-2} is the saturation pump-power density. The net spin polarization is suppressed in a transverse magnetic field B due to the Hanle effect.[1] The Hanle curves we obtained for this sample are shown in Fig. 2(c). They are well described by the Lorentzian

$$S_z = \frac{S_z(W)}{1 + (B/B_{1/2})^2}. \tag{2}$$

Here, $B_{1/2}=\hbar/(g_e\mu_B T_s)$ is the half width at half maximum (HWHM) of the Hanle curve given by the spin lifetime T_s which is connected to optical recombination. The Hanle HWHM $B_{1/2}$ increases with pump-power density W as shown in Fig. 2(d). This behavior is well established for n-GaAs.[1] Upon increasing W, recombination with photogenerated holes provides an additional spin-decay channel resulting in a decrease in the spin lifetime given by[10]

$$B_{1/2} \propto T_s^{-1} = \tau_s^{-1}(1 + W/W_0). \tag{3}$$

Here W_0 defines a characteristic pump-power density and the regime where $W > W_0$ implies strong spin pumping. In the limit of zero power density, T_s is equal to the spin-relaxation time of electrons τ_s and using the well-known electron g factor in GaAs ($g_e=-0.44$) our Hanle data yield an electron-spin relaxation time $\tau_s=(91\pm2)$ ns [Fig. 2(d)].

Figure 2(e) demonstrates the dependence of the Kerr angle θ on the probe energy E_p in zero magnetic field (solid line). Note that the Kerr rotation completely vanishes at $B=5$ mT (in the limit of low pump and probe density, dotted line). In the subsequent experiments, we measure the Kerr angle at a fixed energy of $E_p=1.514$ eV (as indicated by the arrow).

We now describe our results obtained by Kerr microscopy where the laser beams are focused tight enough to resolve spin diffusion. Diffusion of optically injected spins leads to the spatial profiles shown in Fig. 3(a). The dotted line in this figure shows the spin excitation profile as detected by the probe, yielding a net resolution of $\Delta=7.5$ μm. The spatial HWHM $X_{1/2}$ of the scans in the Figure is not constant, as one might naively anticipate, but rises from 14 μm for $W=0.06$ kW cm^{-2} to 23 μm for $W=2.5$ kW cm^{-2}. The broadening partly originates in the modification of the spin-excitation profile in the saturation regime. However, this contribution cannot explain the full observed increase of $X_{1/2}$.[12] Most of the observed behavior can be ascribed to an enhancement of the spin-diffusion length $L_s=\sqrt{D_s\tau_s}$.

The influence of light on spin diffusion is summarized for different probe-power densities in Fig. 3(b). As a general trend, the spin-diffusion length decreases with increasing probe-power density. In order to examine the origin of such a behavior, we plot in Fig. 3(c) the Kerr rotation at the excitation point ($x=0$) as function of pump-power density for several probe-power densities. These dependencies are well fitted by Eq. (1) where the fitting procedure reveals that the saturation pump power density W_S also depends on the probe-power density, following a linear increase [see inset of Fig. 3(c)]. This makes intuitive sense; the faster the spin decay, the stronger spin pumping is required to achieve saturation. The probe beam generates holes introducing an addi-

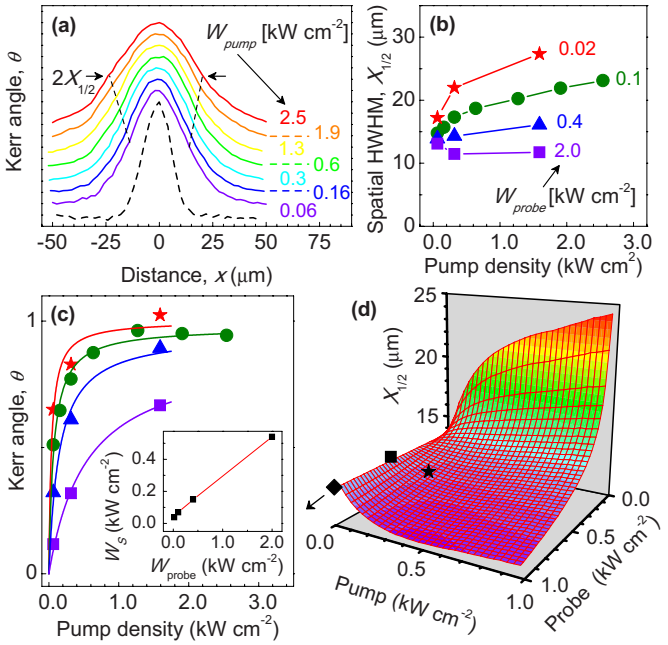

FIG. 3. (Color online) Spin pumping in the diffusive regime. (a) Spatial spin distribution for different pump-power densities W_{pump}. The probe-power density is $W_{\text{probe}}=0.1$ kW cm^{-2}. The dotted curve gives the experimental resolution. (b) Spatial HWHM $X_{1/2}$ vs pump power density for several probe-power densities. (c) Kerr angle at the center of the pump spot ($x=0$) vs pump-power density for several probe-power densities [the same as in panel (b)]. Solid lines are fits to Eq. (1). Inset: saturation pump-power density W_S vs probe-power density W_{probe}. (d) A polynomial interpolation of (b) summarizing the dependence of the spatial HWHM $X_{1/2}$ on pump- and probe-power density. Symbols indicate experimental conditions in various papers: ★—Ref. 3, ■—Ref. 7, and ◆—Ref. 9.

tional spin decay channel. The efficiency of this channel scales with the ratio of the spin-relaxation time and the electron-hole recombination time and it obviously is efficient even at moderate power density. As a consequence, the spin polarization is destroyed and the spin diffusion is suppressed for increasing probe-power density. The overall dependence of the spin-diffusion process on the pump and probe-power density is summarized in Fig. 3(d). In this plot we have included the actual experimental conditions from various recent papers, labeled by symbols. While the influence of the power level used in these works is not very significant, these data have not been taken in the true low perturbation regime.

In order to examine the role of possible heating by light in the increase in $X_{1/2}$, we measured spin diffusion at different temperatures, as shown in Fig. 4(a). In contrast to the results above, we observe a monotonic decrease in $X_{1/2}$ up to $T=100$ K [Fig. 4(b)]. This suggests that optically injected electrons do not only provide a local spin source but also participate in spin transfer over tens of microns.

We now demonstrate how the above effect in combination with weak magnetic fields can be used to locally manipulate the spin flow out of the excitation spot. A two-dimensional (2D) spatial scan in the regime of strong spin pumping $W_{\text{pump}} \gg W_0 (W_{\text{pump}}=1.6$ kW cm$^{-2})$ is shown in Fig. 5(a) for zero magnetic field. In order to minimize the influence of

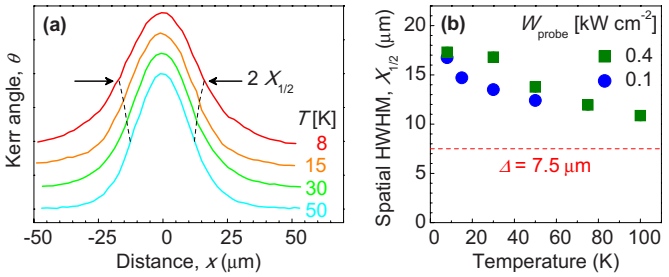

FIG. 4. (Color online) (a) Spatial spin distribution for different temperatures. $W_{\text{pump}}=1.6$ kW cm^{-2} and $W_{\text{probe}}=0.1$ kW cm^{-2}. (b) Spatial HWHM $X_{1/2}$ as function of temperature for two different probe-power densities. The net spatial resolution $\Delta=7.5$ μm is shown by the dotted line.

the probe light, its power density is reduced to $W_{\text{probe}}=0.1$ kW cm^{-2}. When an external magnetic field is applied in the sample plane, the spatial spin distribution changes drastically [Fig. 5(b)]. As clearly seen in Fig. 5(c), the HWHM of the spatial profile $X_{1/2}$ decreases with increasing magnetic field and saturates for $B>5$ mT at the resolution limit of $\Delta=7.5$ μm resulting from the finite sizes of pump and probe spots.

Obviously, the spin gradient $\nabla_s \propto \partial\theta/\partial x$ in Fig. 5 also depends on the in-plane magnetic field. We now concentrate on the spin gradient at the point $x=\Delta$. It has a precise physical meaning; in zero magnetic field $\nabla_s(\Delta)$ is proportional to the spin flow emanating from the injection point due to the diffusion process. We plot in Fig. 5(d) $\partial\theta/\partial x$ obtained at $x=\Delta$ as function of the magnetic field. The data are normalized by their value in zero field. The spin gradient shows a nonmonotonic behavior. For small magnetic fields it increases until its

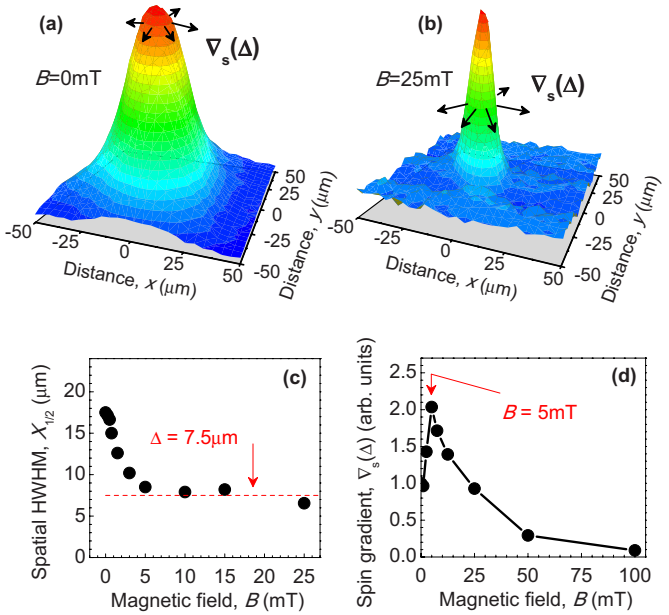

FIG. 5. (Color online) (a) Spatial spin distribution in zero magnetic field. (b) The same in a transverse magnetic field of 25 mT. (c) Spatial HWHM vs magnetic field. (d) Spin gradient $\partial\theta/\partial x \propto \nabla_s$ obtained at a distance $x=\Delta$ vs magnetic field. $W_{\text{pump}}=1.6$ kW cm^{-2} and $W_{\text{probe}}=0.1$ kW cm^{-2}.

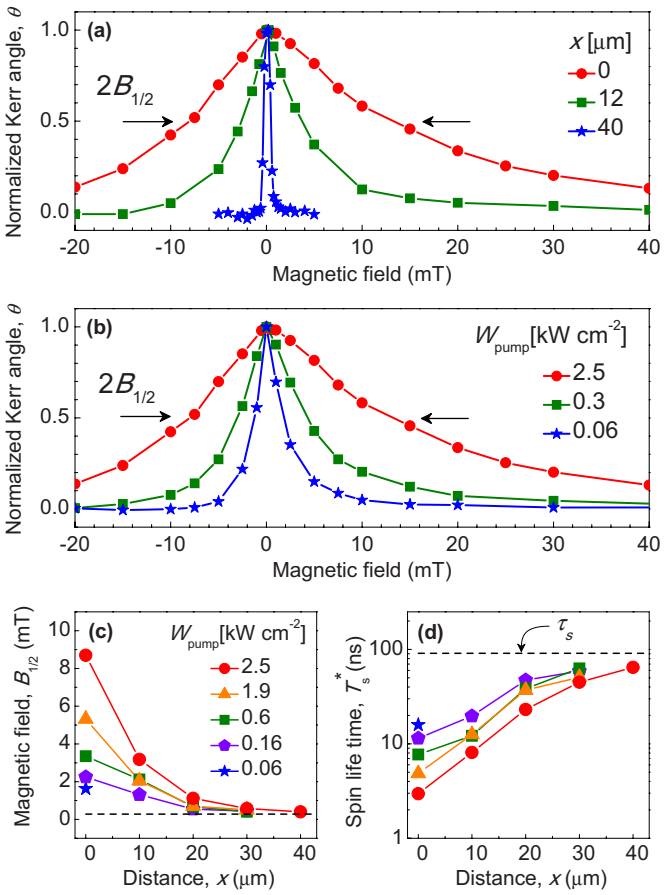

FIG. 6. (Color online) Spatially resolved Hanle effect obtained with W_{probe}=0.1 kW cm^{-2}. (a) Local Hanle curves for different distances x. W_{pump}=2.5 kW cm^{-2}. (b) Local Hanle curves for different pump-power densities W_{pump} at x=0 μm. (c) Spatial dependencies of $B_{1/2}$ for different pump-power densities. (d) Spatial dependence of the apparent spin lifetime T_s^* for different pump-power densities.

value has doubled, then it decreases toward zero in stronger fields. The maximum is achieved at B=5 mT. A possible explanation could be related to the precession of diffusing spins. However, we found from the measurement of local Hanle curves (see Fig. 6) that the effect vanishes with decreasing pump-power density. Therefore, such an explanation is unlikely because the Larmor frequency is independent of the light intensity. This implies that the spin flow from the injection area is indeed enhanced in weak in-plane magnetic fields.

In order to highlight the origin of this effect, we have taken Hanle curves at various positions in the diffusion profile. These data are shown in Fig. 6(a). The small asymmetry of these curves results from the orientation of the optically generated spins under an angle γ=11° with respect to the sample normal (z axis). At the generation point x=0 μm a much higher magnetic field ($2B_{1/2}$=18 mT) is required to suppress the spin polarization than in more distant locations ($2B_{1/2}$=6 mT at x=12 μm and $2B_{1/2}$=0.8 mT at x=40 μm). This strong spatial dependence of the spin lifetime actually scales with illumination power density. As shown in Fig. 6(b), when the pump-power density decreases from W_{pump}=2.5 kW cm^{-2} to W_{pump}=0.06 kW cm^{-2} the width of the local Hanle curves detected at x=0 also reduces from $2B_{1/2}$=18 mT to $2B_{1/2}$=3.2 mT.

The spatial dependencies of $B_{1/2}$ for different pump-power densities are summarized in Fig. 6(c). Remarkably, when the detection point is far away from the injection point (for x>20 μm), $B_{1/2}$ is nearly independent of the pump power and tends toward $B_{1/2}$=0.28 mT, as obtained for low pump-power densities in Fig. 2(d), where spin diffusion can be neglected because of the large illumination area.

The experimental results of Fig. 6(c) can be interpreted in terms of an apparent spin lifetime T_s^*. Despite the Hanle curves in the diffusive regime are not described by the Lorentzian of Eq. (2),[1,2] also in this case the width of the Hanle curves scales with the inverse of the spin lifetime.[13] Hence, we evaluate this apparent spin lifetime using $T_s^* = \hbar/(g_e \mu_B B_{1/2})$. The T_s^* values thus obtained are plotted in Fig. 6(d) as a function of the distance x for different pump-power densities. In case of low pump-power density the apparent spin lifetime is four times shorter at the point of injection (T_s^*<16 ns at x=0 μm) than at distant points (T_s^*>65 ns at x=30 μm). This difference can be related to the "boundary effect.[14]" However, when increasing W_{pump} to 2.5 kW cm^{-2} the apparent spin lifetime decreases down to T_s^*=3 ns at x=0, while for x>20 μm the light has almost no influence on T_s^*. These data clearly demonstrate that illumination induces a spatial variation of the spin lifetime.

Based on the results of Fig. 6 we propose the following physical explanation for the increase of spin flow at low magnetic field presented in Fig. 5(d). In zero field the optically generated spins S_z diffuse away to a distance of the order of the spin-diffusion length L_s resulting in a spin gradient $\nabla_s \propto S_z/L_s$. Outside of the injection area, photogenerated holes are absent and the spin lifetime entering Eq. (3) is equal to the electron-spin relaxation time $T_s^* \approx \tau_s$. Therefore, in relatively weak magnetic fields ($B \sim 5$ mT) the net spin polarization is completely suppressed in this region. Quite the opposite situation prevails inside the injection area when the condition of strong spin pumping ($W_{pump} \gg W_0$) is fulfilled. In this case $T_s^* \ll \tau_s$ and much higher magnetic fields are required to suppress the net spin polarization. As a result, the spin gradient increases in weak magnetic fields according to $\nabla_s \sim S_z/\Delta$. The enhancement factor can be estimated as L_s/Δ. In sufficiently strong magnetic fields the spin polarization inside the injection area is also suppressed ($S_z \to 0$) and the spin gradient decreases to zero. For low pump-power densities ($W \ll W_0$)$T_s^* \approx \tau_s$ according to Eq. (3) and the spin gradient decreases spatially uniformly with increasing magnetic field and the effect disappears.

Summarizing, we used scanning Kerr microscopy to reveal a strong influence of pump and probe on spin transport at the power levels which are frequently assumed to satisfy weak spin pumping conditions. We demonstrate that optical illumination induces spatial variations in the spin lifetime, which in turn can be used to locally control the spin flow when combined with a weak magnetic field.

The authors thank T. Kiessling for valuable discussions. This research was supported by the DFG (program SPP 1285).

*Also at A. F. Ioffe Physico-Technical Institute, RAS, 194021 St. Petersburg, Russia; astakhov@physik.uni-wuerzburg.de

[1] *Optical Orientation*, edited by F. Meyer and B. P. Zakharchenya (North-Holland, Amsterdam, 1984).
[2] R. I. Dzhioev, B. P. Zakharchenya, V. L. Korenev, and M. N. Stepanova, Phys. Solid State **39**, 1765 (1997).
[3] S. A. Crooker and D. L. Smith, Phys. Rev. Lett. **94**, 236601 (2005).
[4] M. Oestreich, J. Hubner, D. Hagele, P. J. Klar, W. Heimbrodt, W. W. Ruhle, D. E. Ashenford, and B. Lunn, Appl. Phys. Lett. **74**, 1251 (1999).
[5] R. Fiederling, M. Keim, G. Reuscher, W. Ossau, G. Schmidt, A. Waag, and L. W. Molenkamp, Nature (London) **402**, 787 (1999).
[6] Y. Ohno, D. K. Young, B. Beschoten, F. Matsukura, H. Ohno, and D. D. Awschalom, Nature (London) **402**, 790 (1999).
[7] S. A. Crooker, M. Furis, X. Lou, C. Adelmann, D. L. Smith, C. J. Palmstrøm, and P. A. Crowell, Science **309**, 2191 (2005).
[8] P. Kotissek, M. Bailleul, M. Sperl, A. Spitzer, D. Schuh, W. Wegscheider, C. H. Back, and G. Bayreuther, Nat. Phys. **3**, 872 (2007).
[9] Y. K. Kato, R. C. Myers, A. C. Gossard, and D. D. Awschalom, Science **306**, 1910 (2004).
[10] H. Hoffmann, G. V. Astakhov, T. Kiessling, W. Ossau, G. Karczewski, T. Wojtowicz, J. Kossut, and L. W. Molenkamp, Phys. Rev. B **74**, 073407 (2006).
[11] S. A. Crooker, M. Furis, X. Lou, P. A. Crowell, D. L. Smith, C. Adelmann, and C. J. Palmstrøm, J. Appl. Phys. **101**, 081716 (2007).
[12] According to Eq. (1) the spin excitation profile is $[1+W_S/W\exp(x^2/\Delta^2)]^{-1}$. As can be inferred from Fig. 3(b), for a probe-power density $W_{\mathrm{probe}}=0.1$ kW cm^{-2} this gives a correction to the HWHM of the spin excitation profile of about 5 μm.
[13] M. I. Dyakonov and V. I. Perel, Fiz. Tekh. Poluprovodn. (S.-Peterburg) **10**, 350 (1976).
[14] H.-A. Engel, Phys. Rev. B **77**, 125302 (2008).